Supplementary Material

Miniaturization of a-Si guided mode resonance filter arrays for near-IR multi-spectral filtering

Ryan C. Ng,[1,a)] Juan C. Garcia,[2] Julia R. Greer,[3] and Katherine T. Fountaine[2]

[1]*Division of Chemistry and Chemical Engineering, California Institute of Technology, Pasadena, California 91125, USA*

[2]*NG Next, Northrop Grumman Corporation, One Space Park, Redondo Beach, California 90278, USA*

[3]*Division of Engineering and Applied Sciences, California Institute of Technology, Pasadena, California 91125, USA*

2D nanopillar array

While the design and discussion in this work is restricted to a 1D design, all the ideas here are fully applicable to a 2D design should a polarization-independent response be desired at normal incidence using an array of pillars or cubes with mirrors on all four sides. To illustrate this idea, in Figure S1 we present a proof-of-concept design in 2D that has not been optimized, but still exhibits the GMR rapid spectral variation. Figure S1(a) presents a schematic of this design, with Al mirrors on only two sides, and Figure S1(b) shows the associated reflection spectrum. This array has geometric parameters h = 150 nm, a = 800 nm, f = 0.5, and s = 300 nm for a 7x7 array of a-Si nanopillars embedded in SiO_2 with Al mirrors. The spectral characteristics can be significantly improved through optimization of the geometric parameters. While mirrors are required on all four sides for polarization-independence, the ability to miniaturize this design and visualize the GMR with mirrors only along one direction further support the GMR mechanism.

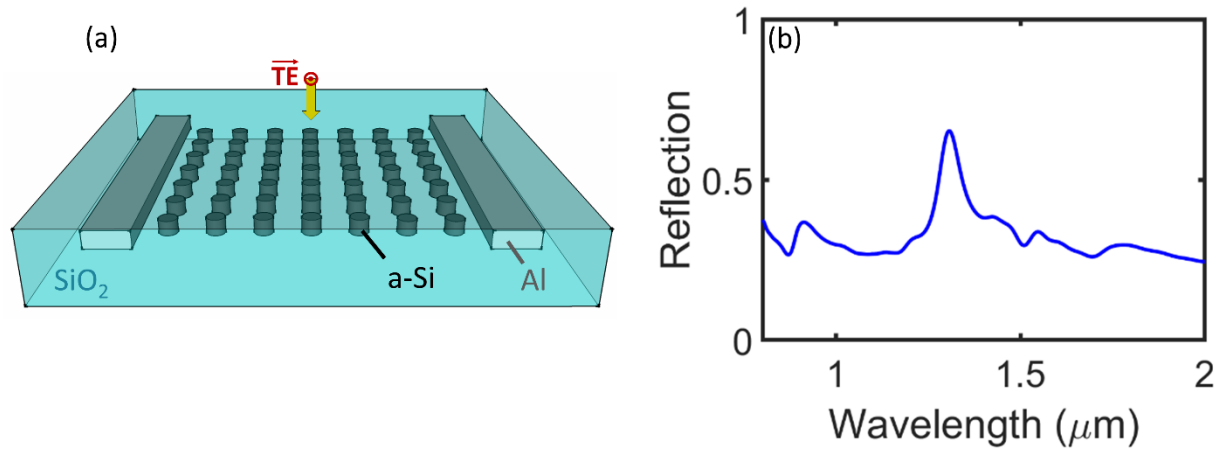

FIG. S1. GMR in compact finite 2D design incorporating mirrors. (a) Schematic of a 2D design incorporating mirrors only along two boundaries for an array with geometric parameters h = 150 nm, a = 800 nm, f = 0.5, and s = 300 nm for a 7x7 array of a-Si nanopillars embedded in SiO_2 with Al mirrors. (b) Associated reflection spectrum calculated in FDTD demonstrating a non-optimized proof-of-concept of the compact finite array design and ability to observe the GMR utilizing a 2D array should polarization-independence be desired.

Number of periods required to obtain desired spectral characteristics

For comparison, to quantify the advantage of incorporating a mirror in terms of filter footprint, FDTD simulations were done to determine the number of periods required in a finite design that does not incorporate any mirrors to match the amplitude of other higher-performance designs (Figure S2). Figure S2(a) compares the performance of a 17-period finite mirrorless design with the 7-period finite design incorporating mirrors proposed in this work. Figure S2(b) compares the performance of a 141-period finite design that does not incorporate mirrors with an infinite design. While it is possible to obtain high spectral resolution and high signal-to-noise ratio spectral peaks using GMR filter designs that do not incorporate any kind of reflective boundaries, this comes at the cost of extremely large lateral footprints.

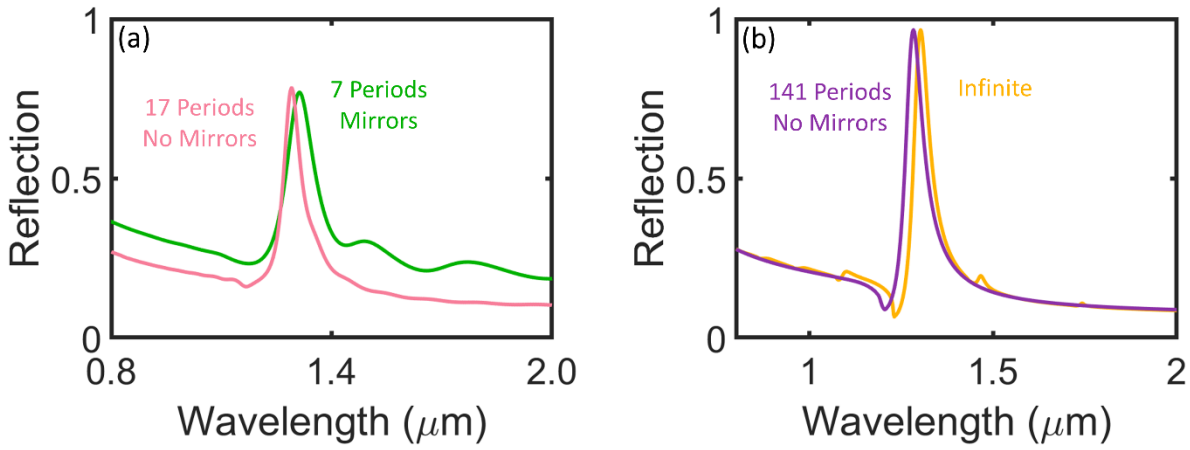

FIG. S2. FDTD simulations comparing spectra between designs that incorporate mirrors and designs that do not incorporate mirrors, indicating the number of periods required in a mirrorless design to match the performance of other designs in terms of peak amplitude. (a) Comparison between the finite 7-period design that incorporates mirrors in this work (green) with a finite 17-period design that does not incorporate mirrors (pink). (b) Comparison between an infinite design (yellow) and a finite 141-period design that does not incorporate mirrors (purple).

Effect of varying period in finite GMR design

The effect of varying the number of periods in the finite design incorporating mirrors is shown in FDTD calculated spectra in Figure S3. With a lower number of periods, the amplitude of the peak decreases, the FWHM broadens, and background noise increases. However, depending on the specific signal-to-noise that may be desired in the final imaging device, a filter incorporating only 3 periods still exhibits a GMR that may be useful if the lower signal-to-noise ratio and lower spectral resolution is acceptable in a particular application.

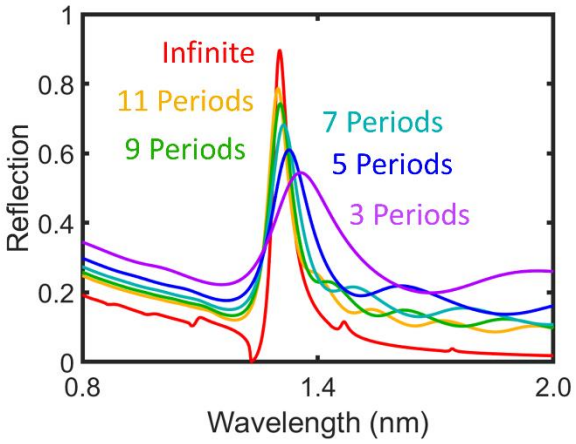

FIG. S3. FDTD generated reflection spectra demonstrating the effect of varying the number of periods and varying filter footprint in the finite design incorporating mirrors. As the number of periods decreases, the amplitude decreases and the bandwidths broaden with increased background noise.

Spectral characteristics of arrays

Table S1 shows the spectral characteristics of the fabricated arrays measured experimentally compared to experiment. We observe FWHM values from 140.5 to 205.1 nm in experiment, and from 102.7 to 120.6 nm in simulation (overestimation of actual FWHM and underestimation of their performance due to defining the FWHM as half of the peak reflection due to the asymmetric resonance, defined in the main text). For example, to calculate the FWHM for the 731 nm period array in simulation, we find the bandwidth at half of the reflection amplitude (82.6/2), which results in a bandwidth of 102.7 nm. This is to avoid ambiguity since the baseline has a slightly different amplitude on either side of the asymmetric resonance. Our definition of FWHM causes a significant overestimation of the bandwidth of the 881 nm array in experiment. The transmission dips are as low as 58.1% experimentally, compared to 17.4% in simulation. We attribute this efficiency loss to fabrication imperfections, experimental normalization, and alignment errors in fabrication and measurement (angle and polarization).

Table S1. Spectral characteristics for each array in {experiment / simulation} for variable periodicity with 7 periods. The color scheme is consistent with that in Figure 3.

Period (nm)	Peak Position (nm)	Reflection Amplitude	FWHM (nm)
731	1180 / 1176	41.9 / 83.0	140.5 / 103.6
781	1230 / 1244	39.0 / 79.4	157.5 / 106.2
831	1300 / 1312	34.0 / 75.4	143.9 / 110.4
881	1350 / 1381	32.5 / 71.1	205.1 / 116.0
931	1400 / 1449	23.0 / 66.7	188.6 / 122.7

Top down schematic of filter array and surrounding reflective frame

Rather than patterning and depositing two rectangular blocks for the mirrors as suggested by Figure 1(a), we surround the filter with an Al frame. This Al frame now serves two purposes: 1) to allow the GMR to reflect back to approximate infinite periodicity and 2) to enable normalization during measurements through the array. Transmission through mirror frames matching the area of the sample but with no patterned area was measured to properly normalize the power transmitted through the patterned sample area, though only reflective mirrors on two sides of the array are required to observe the laterally propagating GMR in the finite array. An aerial schematic of this layout is shown in Figure S4 and the dimensions of the frame and distances from the filter are indicated. The a-Si array is indicated in red and the surrounding Al frame in dark blue. This frame is discontinuous with slits in the frame for ease of experimental lift-off. Frames of the same lateral dimensions were fabricated without gratings for normalization of the transmission measurements.

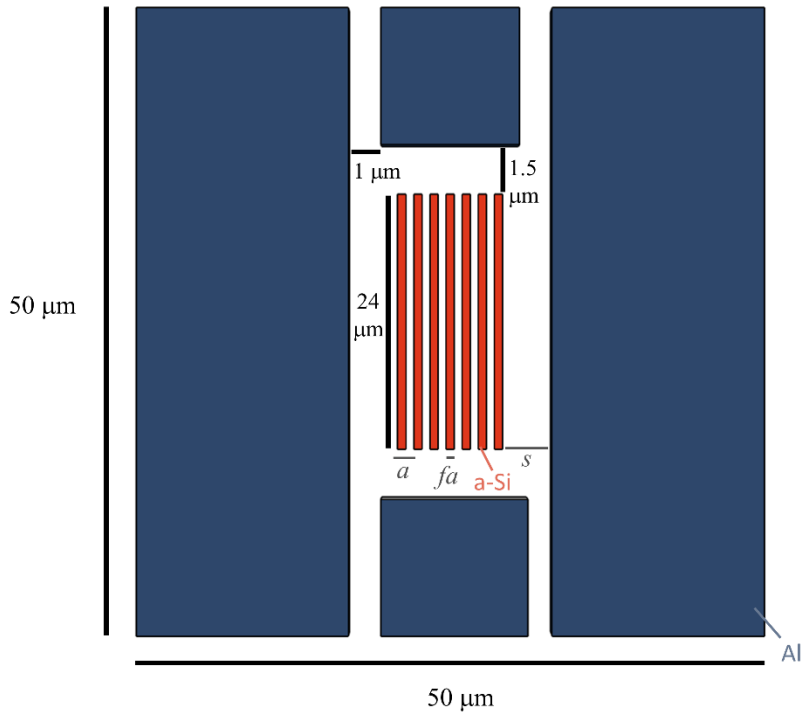

FIG. S4. Top-down schematic of the 7 period a-Si filter array and surrounding Al mirror/frame. The frame is introduced for ease of normalization during measurements. Slits are included in the frame for ease of lift-off during fabrication. The array of a-Si slabs has variable periodicity, *a*, fill fraction, *f*, and spacer region, *s*. Dimensions for the frame, slits, distance from the array, and lateral length of the array slabs are indicated in the figure. This schematic is not to scale.

Ellipsometry

Ellipsometry data was obtained (Figure S5) for a 100 nm thick film of a-Si deposited by PECVD at 200^{o}C, 800 mTorr, and 10 W with 250 sccm of 5% SiH_4 diluted in Ar. This n,k data was used in in the FDTD simulations to model a-Si.

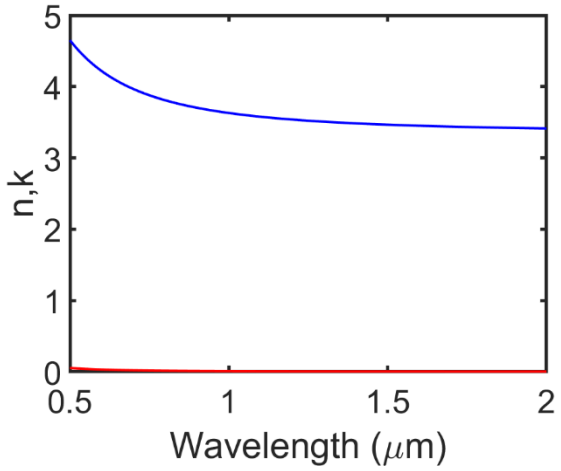

FIG. S5. Raw n and k data for a-Si determined from ellipsometry.

Fresnel Correction

This calculation allows for the additional top and bottom interfaces of the glass substrate to be accounted for, that are not otherwise accounted for in FDTD simulations. The calculation can be done for a fixed number of layers, and then generalized to an arbitrary number of layers. First, we assume we have a homogeneous film of a single material in air (i.e. air-film-air with each layer numbered as layers 0, 1, and 2, respectively). This stack is schematically shown in Figure S6. R_A is the amplitude of the wave reflected directly from the top surface of the film, R_B is the amplitude of the wave reflected from the bottom surface of the film that transmits back through the top surface, R_C is the wave that reflects from the bottom surface, then internally reflects again off the top surface then bottom surface, before transmitting through the top surface, and so on. Then, R_{ij}, T_{ij}, r_{ij} are the reflectance, transmittance, and reflection coefficients at each interface between each layer, respectively. We define:

$$R_{01} = {r_{01}}^2$$

At normal incidence:

$$R_{01} = \left(\frac{n_0 - n_1}{n_0 + n_1}\right)^2$$

As R_A is the reflectance off the top interface,

$$R_A = R_{01}$$

Then,

$$R_B = T_{01}R_{12}T_{10}$$

$$R_C = T_{01}R_{12}R_{10}R_{12}T_{10}$$

More generally, to describe the reflectance out of the top surface after *m* internal reflections off the back-side of the film for $\alpha \geq 1$:

$$R_m = T_{01}T_{10}R_{12}{}^{\alpha}R_{10}{}^{\alpha-1}$$

The total reflectance out of the top surface is the sum of all of these R_m terms that transmit from the film to the top surface:

$$R_{tot} = \sum R_m = R_{01} + T_{01}T_{10}R_{12}\sum_{\alpha=0}^{\infty} R_{12}{}^{\alpha}R_{10}{}^{\alpha}$$

This is a geometric series:

$$R_{tot} = R_{01} + T_{01}T_{10}R_{12}\left(\frac{1}{1-R_{12}R_{10}}\right)$$

For normal incidence, TE and TM polarization are the same, i.e. $T = 1 - R$ for TE, but $R_{TE} = R_{TM}$. We also utilize $R_{ij} = -R_{ji}$. For a 3-layer air-film-air stack, R_{02} describes the total reflectance in this system considering all interfaces. Simplifying:

$$R_{tot} = R_{02} = \frac{R_{01} + R_{12}}{1 + R_{12}R_{01}}$$

This result can similarly be generalized to a different number of layers. For a stack of 4 layers:

$$R_{\text{tot}} = R_{03} = \frac{R_{01} + \left(\frac{R_{12} + R_{23}}{1 + R_{23}R_{12}}\right)}{1 + \left(\frac{R_{12} + R_{23}}{1 + R_{23}R_{12}}\right) R_{01}}$$

This is the expression utilized in this work for a 4-layer film of air-glass-glass-air, where the FDTD simulated spectrum represents R_{12}, the reflection at the interface between the glass-glass layers.

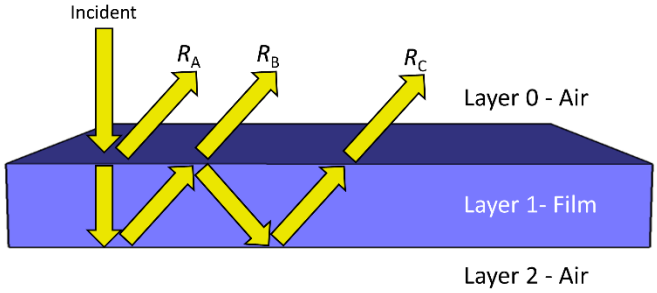

FIG. S6. Schematic of Fresnel reflection through the interfaces of a single slab of homogeneous material. Here, layer 0 and layer 2 are air, though this can be generalized to any cover or substrate. R_A is the amplitude of the wave reflected directly from the top surface of the film, R_B is the amplitude of the wave reflected from the bottom surface of the film that transmits back through the top surface, R_C is the wave that reflects from the bottom surface, then internally reflects again off the top surface then bottom surface, before transmitting through the top surface, and so on.

Methods

Fabrication: The filter arrays were fabricated using a top-down methodology on a glass substrate. Approximately 64 nm of a-Si was deposited onto the substrate by PECVD at 200ºC, 800 mTorr, and 10 W with 250 sccm of 5% SiH_4 diluted in Ar for 2 minutes and 18 seconds. The thickness deposited in PECVD dictates the height of the a-Si slabs in the array. Prior to all electron beam lithography writes in the fabrication process, a sacrificial layer (a solution of poly(4-styrenesulfonic acid) mixed with 1% by volume of Triton X-100 surfactant) was spin-coated above the resist at 3000 rpm and baked at 90ºC for 3 minutes, followed by 10 nm of electron beam

evaporated Au for charge dissipation. The sacrificial layer gold was removed following EBL in water and developed as normal. Ti alignment markers (h = 200 nm) were created by first patterning in polymethyl methacrylate (PMMA) 950 A8 positive-tone electron beam resist with a Raith 5000+ electron beam writer at 100 kV, developing in methyl isobutyl ketone:isopropanol (MIBK:IPA) in a 1:3 ratio for 90 seconds, and then depositing Ti in electron beam evaporation and lifting off. The next EBL write utilized MaN-2403 negative-tone electron beam resist applied onto the a-Si. The grating slabs were then exposed in an aligned write to the Ti markers and are 21 μm each in length. Following electron beam exposure, the pattern was developed in MF-319 for 40 seconds and the pattern was transferred into the a-Si layer with a pseudo-Bosch SF_6/C_4F_8 etch with ICP-RIE at 15 ºC with 40 W ICP power, 1500 W forward power, 26 sccm of SF_6 and 35 sccm of C_4F_8. The MaN-2403 resist mask was removed by cleaning in an oxygen plasma for 10 minutes (10 mtorr and 80 W with 20 sccm O_2). Finally, the mirrors were aligned and patterned with PMMA 950 A4 and developed in 1:3 MIBK:IPA for 90 seconds, and a 65 nm thick layer of Al that dictated the mirror height was deposited in electron beam evaporation and subsequently lifted-off. Rather than patterning and depositing two rectangular blocks for the mirrors as suggested by Figure 1(a), we surround the filter with an Al frame. This frame is the length of the filter and spacer regions in one lateral direction perpendicular to the grating beams, and 24 μm in the other lateral direction parallel to the grating beams (Figure S4). It is discontinuous with slits in the frame for ease of experimental lift-off. Frames of the same lateral dimensions were fabricated without gratings for normalization of the transmission measurements. The resulting filter was in-filled with 500 nm of methylsiloxane based spin-on glass solution (Filmtronics 500F).

Measurement: Measurements were made with a Fianium white light source coupled to a near-IR monochromator with Ge photodetectors and a 20X Mitutuyo objective with a range from 480-

1800 nm. This objective allowed focusing of the spot size down to ~10 μm. Transmission measurements were taken from 1100 to 1600 nm spaced evenly 10 nm apart from one another. To properly normalize to the power transmitted through the patterned sample area, transmission through mirror frames matching the area of the sample but with no patterned area was measured. To account for any power fluctuations between the measurement of the sample and the frame, a pair of Ge photodetectors simultaneously recorded the intensity of the beam transmitting through the sample, I_{ref}, and the intensity of the incident beam, I_{inc}, using a beamsplitter prior to the objective. The transmissivity of the sample, T, was then calculated by:

$$T = \left(\frac{I_{\text{ref}}}{I_{\text{inc}}}\right)_{\text{sample}} \left(\frac{I_{\text{inc}}}{I_{\text{ref}}}\right)_{\text{frame}}$$

*Simulatio*n: Full-field, 2D simulations were computed with Lumerical FDTD, a commercial electromagnetics software package. For infinite simulations (Figures 1(b) and 1(c)) and crosstalk simulations (Figure 4), periodic boundary conditions were used on the lateral boundaries to reduce the simulation region and emulate infinite periodicity. For finite simulations (Figures 1(b), 1(d), 1(e), 2, and 3), perfectly matched layers were used for the lateral boundaries as an artificial absorbing region to emulate infinite space. In all cases, perfectly matched layers were used for the axial boundaries. For the polarization, the E-field is parallel to the direction of the length of the grating slabs. For the materials in the simulation, Palik data was used for Al and SiO_2 and ellipsometric data was used for a-Si (Figure S5). A finer override mesh was applied over the a-Si slabs with mesh sizes <5% of the height and width of the slabs. The spectra in this work utilized single broadband (800-2000 nm) simulations. A Fresnel correction was applied to all simulations to account for interfaces that were not included in simulation (Figure S6).